AFRL-SR-AR-TR-10-0047

REPORT DOCUMENTATION PAGE

Public reporting burden for this collection of information is estimated to everage 1 hour per response, including the time for reviewing instructions, searching existing data sources, gathering end maintaining the data needed, and completing end reviewing this collection of information. Send comments regarding this burden estimate or eny other espect of this collection of information, including suggestions for reducing this burden to Department of Defense, Washington Headquarters Services, Directorate for Information Operations end Reports (0704-0188), 1215 Jefferson Davis Highwey, Suite 1204, Arlington, VA 22202-4302. Respondents should be eware thet notwithstanding eny other provision of lew, no person shell be subject to eny penalty for failing to comply with e collection of informetion if it does not display a currently valid OMB control number. **PLEASE DO NOT RETURN YOUR FORM TO THE ABOVE ADDRESS.**

1. REPORT DATE *(DD-MM-YYYY)*	2. REPORT TYPE	3. DATES COVERED *(From - To)*
12/27/2009	FINAL PERFORMANCE REPORT	4/01/2006-9/30/2009

4. TITLE AND SUBTITLE

Effect of Nanoscale Fillers on the Local Mechanical Behavior of Polymer Nanocomposites

5a. CONTRACT NUMBER

5b. GRANT NUMBER
FA9550-06-1-0140

5c. PROGRAM ELEMENT NUMBER

6. AUTHOR(S) IOANNIS CHASIOTIS

Aerospace Engineering, U. Illinois at Urbana-Champaign, M/C 236
306 Talbot Lab, 104 South Wright St., Urbana, IL 61801

5d. PROJECT NUMBER

5e. TASK NUMBER

5f. WORK UNIT NUMBER

7. PERFORMING ORGANIZATION NAME(S) AND ADDRESS(ES)

UNIVERSITY OF ILLINOIS
Aerospace Engineering
104 South Wright St.
Urbana, IL 61801

8. PERFORMING ORGANIZATION REPORT NUMBER

9. SPONSORING / MONITORING AGENCY NAME(S) AND ADDRESS(ES)

Air Force Office of
Scientific Research (AFOSR)
Program: Mechanics of
Multifunctional Materials and
Microsystems

10. SPONSOR/MONITOR'S ACRONYM(S)
Program Manager:
Dr. B.L. Lee

11. SPONSOR/MONITOR'S REPORT NUMBER(S)

12. DISTRIBUTION / AVAILABILITY STATEMENT
DISTRIBUTION A

20100226332

13. SUPPLEMENTARY NOTES

14. ABSTRACT

In this research program we investigated (a) the effective and local mechanical and fracture behavior of EPON epoxy with nanoscale fumed silica particles, and (b) the mechanical and interfacial properties of individual vapor grown carbon nanofibers (VGCNFs) embedded in EPON epoxy. Local Atomic Force Microscopy/Digital Image Correlation (AFM/DIC) measurements showed strain localization and matrix yielding in the vicinity of 100-nm silica particles, which reduced the composite stiffness. The tensile strength of all silica composites was independent of particle size and weight fraction due to strong particle bonding and failure initiation in the matrix, while the critical mode I stress intensity factor of 12-nm silica composites increased by as much as 35% for 15 wt.% silica. We also conducted experiments on the mechanical and failure response of VGCNFs by a MEMS mechanical testing platform. Their mechanical strength averaged 2.74 - 3.34 GPa for different fabrication conditions, with as-fabricated VGCNFs having the widest flaw population which was reduced significantly upon heat treatment. The elastic modulus of as received and heat-treated VGCNFs averaged 180 and 250 GPa, respectively, which is significantly higher than reports from previous 'indirect' experiments. The strength of VGCNF-Epon 828 matrix interfaces was also quantified for the first time by novel nanoscale fiber pull-out experiments. The interfacial shear strength (IFSS) of as fabricated VGCNFs was 111±32 MPa and was reduced to 66±10 MPa after heat treatment. Finally, surface functionalization of heat treated VGCNFs restored their IFSS to 214±10 MPa.

UNIVERSITY OF ILLINOIS
AEROSPACE ENGINEERING

FINAL PERFORMANCE REPORT

Reporting Period: 4/01/2006 - 9/30/2009

Effect of Nanoscale Fillers on the Local Mechanical Behavior of Polymer Nanocomposites

PI: Ioannis Chasiotis

Aerospace Engineering
University of Illinois at Urbana-Champaign
Talbot Lab, 104 S. Wright Street, Urbana, IL 61801
Telephone: (217) 244-1474, Fax: (217) 244-0720, E-mail: chasioti@illinois.edu

AFOSR GRANT # FA9550-06-1-0140

Program Manager: Dr. B.L. Lee

DECEMBER 2009

REPORT DOCUMENTATION PAGE

Form Approved
OMB No. 0704-0188

Public reporting burden for this collection of information is estimated to average 1 hour per response, including the time for reviewing instructions, searching existing data sources, gathering and maintaining the date needed, end completing end reviewing this collection of information. Send comments regarding this burden estimate or eny other aspect of this collection of informetion, including suggestions for reducing this burden to Department of Defense, Washington Headquerters Services, Directorate for Information Operations end Reports (0704-0188), 1215 Jefferson Davis Highway, Suite 1204, Arlington, VA 22202-4302. Respondents should be aware that notwithstanding any other provision of law, no person shell be subject to any penelty for failing to comply with a collection of informetion if it does not display e currently valid OMB control number. **PLEASE DO NOT RETURN YOUR FORM TO THE ABOVE ADDRESS.**

1. REPORT DATE *(DD-MM-YYYY)*	2. REPORT TYPE	3. DATES COVERED *(From - To)*
12/27/2009	FINAL PERFORMANCE REPORT	4/01/2006-9/30/2009

4. TITLE AND SUBTITLE

Effect of Nanoscale Fillers on the Local Mechanical Behavior of Polymer Nanocomposites

5a. CONTRACT NUMBER

5b. GRANT NUMBER
FA9550-06-1-0140

5c. PROGRAM ELEMENT NUMBER

6. AUTHOR(S) IOANNIS CHASIOTIS

Aerospace Engineering, U. Illinois at Urbana-Champaign, M/C 236
306 Talbot Lab, 104 South Wright St., Urbana, IL 61801

5d. PROJECT NUMBER

5e. TASK NUMBER

5f. WORK UNIT NUMBER

7. PERFORMING ORGANIZATION NAME(S) AND ADDRESS(ES)

UNIVERSITY OF ILLINOIS
Aerospace Engineering
104 South Wright St.
Urbana, IL 61801

8. PERFORMING ORGANIZATION REPORT NUMBER

9. SPONSORING / MONITORING AGENCY NAME(S) AND ADDRESS(ES)

Air Force Office of
Scientific Research (AFOSR)
Program: Mechanics of
Multifunctional Materials and
Microsystems

10. SPONSOR/MONITOR'S ACRONYM(S)
Program Manager:
Dr. B.L. Lee

11. SPONSOR/MONITOR'S REPORT NUMBER(S)

12. DISTRIBUTION / AVAILABILITY STATEMENT

13. SUPPLEMENTARY NOTES

14. ABSTRACT

In this research program we investigated (a) the effective and local mechanical and fracture behavior of EPON epoxy with nanoscale fumed silica particles, and (b) the mechanical and interfacial properties of individual vapor grown carbon nanofibers (VGCNFs) embedded in EPON epoxy. Local Atomic Force Microscopy/Digital Image Correlation (AFM/DIC) measurements showed strain localization and matrix yielding in the vicinity of 100-nm silica particles, which reduced the composite stiffness. The tensile strength of all silica composites was independent of particle size and weight fraction due to strong particle bonding and failure initiation in the matrix, while the critical mode I stress intensity factor of 12-nm silica composites increased by as much as 35% for 15 wt.% silica. We also conducted experiments on the mechanical and failure response of VGCNFs by a MEMS mechanical testing platform. Their mechanical strength averaged 2.74 - 3.34 GPa for different fabrication conditions, with as-fabricated VGCNFs having the widest flaw population which was reduced significantly upon heat treatment. The elastic modulus of as received and heat-treated VGCNFs averaged 180 and 250 GPa, respectively, which is significantly higher than reports from previous 'indirect' experiments. The strength of VGCNF-Epon 828 matrix interfaces was also quantified for the first time by novel nanoscale fiber pull-out experiments. The interfacial shear strength (IFSS) of as fabricated VGCNFs was 111±32 MPa and was reduced to 66±10 MPa after heat treatment. Finally, surface functionalization of heat treated VGCNFs restored their IFSS to 214±10 MPa.

15. SUBJECT TERMS					
16. SECURITY CLASSIFICATION OF:			17. LIMITATION OF ABSTRACT	18. NUMBER OF PAGES	19a. NAME OF RESPONSIBLE PERSON Ioannis Chasiotis
a. REPORT unclassified	b. ABSTRACT unclassified	c. THIS PAGE unclassified		28	19b. TELEPHONE NUMBER *(include area code) (217) –244-1474*

Standard Form 298 (Rev. 8-98)
Prescribed by ANSI Std. Z39.18

Acknowledgements

The PI and his graduate students, Ms. Qi Chen and Mr. Tanil Ozkan, supported by this program gratefully acknowledge the support by the Air Force Office of Scientific Research (AFOSR) through grant FA9550-06-1-0140 and Dr. B.L. Lee as the program manager. The authors thank their collaborators Drs. A. Roy and C. Chen at the Wright Patterson Air Force Base for providing the samples for the first part of the work conducted under this research grant.

Final Progress Summary

To: technicalreports@afosr.af.mil

Subject: Annual Progress Statement to Dr. B.L. Les Lee

Grant Title: Effect of Nanoscale Fillers on the Local Mechanical Behavior of Polymer Nanocomposites

Grant #: FA9550-06-1-0140

Reporting Period: 4/01/2006 - 9/30/2009

Program Accomplishments:

In this research program we investigated (a) the effective and local mechanical and fracture behavior of EPON epoxy with nanoscale fumed silica particles, and (b) the mechanical and interfacial properties of individual vapor grown carbon nanofibers (VGCNFs) embedded in EPON epoxy. Local Atomic Force Microscopy/Digital Image Correlation (AFM/DIC) measurements showed strain localization and matrix yielding in the vicinity of 100-nm silica particles, which reduced the composite stiffness. The tensile strength of all silica composites was independent of particle size and weight fraction due to strong particle bonding and failure initiation in the matrix, while the critical mode I stress intensity factor of 12-nm silica composites increased by as much as 35% for 15 wt.% silica. We also conducted experiments on the mechanical and failure response of VGCNFs by a MEMS mechanical testing platform. Their mechanical strength averaged 2.74 - 3.34 GPa for different fabrication conditions, with as-fabricated VGCNFs having the widest flaw population which was reduced significantly upon heat treatment. The elastic modulus of as received and heat-treated VGCNFs averaged 180 and 250 GPa, respectively, which is significantly higher than reports from previous 'indirect' experiments. The strength of VGCNF-Epon 828 matrix interfaces was also quantified for the first time by novel nanoscale fiber pull-out experiments. The interfacial shear strength (IFSS) of as fabricated VGCNFs was 111±32 MPa and was reduced to 66±10 MPa after heat treatment. Finally, surface functionalization of heat treated VGCNFs restored their IFSS to 214±10 MPa.

Refereed Publications:

1. Q. Chen, I. Chasiotis, A. Roy, C. Chen, "Nanoscale Strain Measurements in Polymer Nanocomposites", *Proceedings of the Materials Research Society* **977E**, (2007).
2. Q. Chen, I. Chasiotis, C. Chen, A. Roy, "Nanoscale and Effective Mechanical Behavior and Fracture of Silica Nanocomposites," *Composites Science and Technology* **68** (15-16), pp. 3137-3144, (2008).
3. T. Ozkan, M. Naraghi, I. Chasiotis, "Mechanical Properties of Vapor Grown Carbon Nanofibers," *Carbon* **48**, pp. 239-244, (2010).
4. T. Ozkan, Q. Chen, I. Chasiotis, "Interfacial Strength of Individual Vapor Grown Carbon Nanofibers in EPON Epoxy", to be submitted to *Composites Science and Technology,* (2010).

Degree Theses:

1. Q. Chen, "Local and Effective Mechanical Properties of Polymer Nanocomposites", PhD. Dissertation, University of Illinois at Urbana-Champaign, 2009.
2. T. Ozkan, "Mechanical and Interfacial Properties of Carbon Nanofibers for Polymer Nanocomposites", M.S. Dissertation, University of Illinois at Urbana-Champaign, 2009.

Interactions and Transitions to National and Government Laboratories

Collaboration that will lead to data transfer to researchers at Wright Patterson Air Force Base: Collaborators Drs. A. Roy (AFRL) and C. Chen (UDRI).

Changes in research objectives, if any: None

Change in AFOSR program manager, if any: None

Extensions granted or milestones slipped, if any: None

DETAILED TECHNICAL DESCRIPTION OF RESEARCH

This final report presents the scientific and technical findings obtained under the support of this AFOSR grant. The report is divided in two sections: The first section focuses on the local mechanics of silica particle nanocomposites, while the second section presents experiments on the mechanical and failure behavior of different grades of vapor grown carbon nanofibers (VGCNFs) and their interfacial adhesion to epoxy matrices by a novel MEMS-based experimental method.

1. LOCAL DEFORMATION MECHANICS OF SILICA NANOCOMPOSITES

1.1. Materials and Experimental Methods

Composite plates were fabricated at WPAFB with cross-linked EPON 862 (diglycidylbisphenol-F) with curing agent W (diethyltoluenediamine) and 12-nm or 14-nm fumed silica nanoparticles. The 12-nm particles (termed primary particles) were incorporated at weight fractions of 1 - 15 wt.%. Composites where also fabricated with agglomerates of 14-nm silica particles, which are termed secondary particles. These agglomerates had 100 nm effective diameter, relatively tight size distribution, and good dispersion. The weight fractions of composites with secondary silica particles were 0.6 wt.%, 3 wt.%, and 5 wt.%.

Preparation of 100 nm aggregated silica nanoparticles was conducted by dispersing 14-nm spherical silica nanoparticles (fumed silica powder, Aldrich) in Epon 862 by high-shear and ultrasonication, and curing with curing agent W. Preparation of 12-nm individually dispersed silica was done by their dispersion (MEK-ST suspension, Nissan Chemicals) in Epon 862 by ultrasonication, followed by curing with curing agent W. Processing of the two material systems was similar but differences in dispersion were due to the different source of silica nanoparticles, i.e. fumed silica powder (Aldrich) vs. nanoparticles in suspension (Nissan Chemicals).

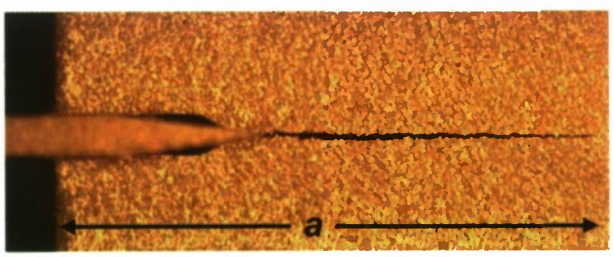

Figure 1. Sharp crack with length *a*, generated by a razor blade at the end of a machined notch [1].

For fracture experiments, single edge notched tension (SENT) specimens (50×10×2 mm) were machined from cast plates. A 1-mm deep and 0.2-mm wide notch with 60° notch tip angle was machined in the middle of each specimen. The notched samples were mounted on a custom-made apparatus where a razor blade was used to generate a natural crack as an extension of the notch root. Pre-crack generation was well controlled, as the razor initiated the crack due to the opening moment applied by the blade edges. An image of the machined notch with a sharp crack is shown in Figure 1. Of the methods attempted to generate

straight pre-cracks (fatigue a notch, specimen freeze, etc.) this method provided the most consistent cracks.

1.2. Experimental Apparatus and Measurement Method

A mechanical testing apparatus was built and implemented under a commercial AFM to obtain *in situ* local mechanical deformations at the scale of the 100-nm particles. The tensile apparatus was integrated with two high-resolution optical microscopes: a horizontal microscope to image the specimen sidewalls, and a vertical microscope to record images of the top surface of the specimen. Digital Image Correlation (DIC) was then applied to compute the stress-strain curves from optical images under quasi-static tensile loading. The effective property measurements yielded the composite properties, which were then related to the local mechanical behavior as deduced from local measurements. All tests were conducted at approximately 10^{-3} s^{-1} strain rate. The specimens were loaded at several increments of stress and the topographic, photodetector signal, and phase AFM images were collected from the center of the specimen gauge section with 512×512 pixel resolution and physical dimensions of 3×3 μm^2. AFM imaging was conducted for composites with 3 wt.%, 100-nm and 5 wt.%, 100-nm silica. At the same time, the effective composite strain was measured optically. The mode-I fracture tests with 12-nm particles were carried out by a tabletop universal testing machine (Model ElectroForce 3200, Bose Corporation) at a rate of 0.12 mm/min. Multiple experiments for each composite type were conducted to establish sufficient statistics.

1.3. Results and Discussion

1.3.a. Effective Mechanical Behavior

Example engineering stress-strain plots for composites with 12-nm and 100-nm silica, are shown in Figures 2(a,b). At least three specimens of each composite sample were tested. Each plot includes two curves for the epoxy with the largest and smallest epoxy strengths that were recorded. The composite elastic moduli were calculated by linear fitting of the initial portion of each curve at strains <0.3%. At the millimeter scale, and at strains larger than 3%, all samples developed localization bands normal to the applied loading followed by microcracking. Thus, sample softening observed at strains larger than 3% was due to microcracking that did not relate to true material deformation. To separate this effect, all engineering stress-strain plots are presented until 3% strain. The ultimate strain for most samples ranged between 7-10% with the smallest values obtained at the largest particle weight fractions.

Compared to the modulus of the epoxy, E=3.09 *GPa*, the composite modulus of 12-nm silica composites, Figure 3(a), increased monotonically with weight fraction (see insert). The Poisson's ratio, on the other hand, was 0.38 and it was independent of particle weight fraction. On the contrary, composites with 100-nm silica particles showed large increase in their modulus at 0.6 wt.%, which then decreased with increasing weight fraction, Figure 3(b). This reduction in modulus may be explained by local matrix yielding at small applied stresses, as will be evidenced in the AFM experiments in the next section. By virtue of purely geometrical

considerations, the interparticle spacing can be related to the particle volume fraction, v_p, and the particle diameter, d, by [2]

$$r = d\left[\sqrt[3]{\frac{\pi}{6v_p}} - 1\right] \tag{1}$$

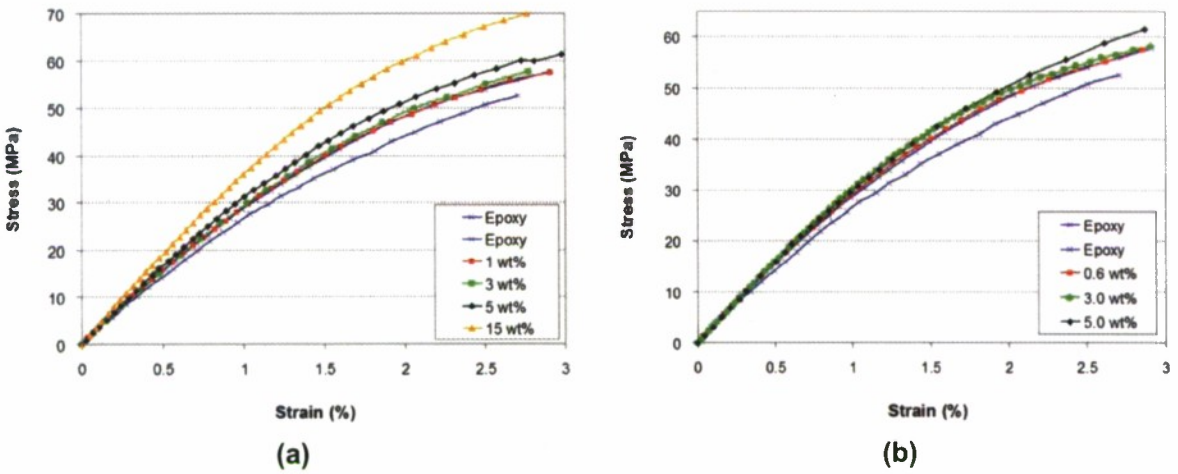

Figure 2. Engineering stress *vs.* strain of the control epoxy and the polymer nanocomposites with **(a)** 12-nm, and **(b)** 100-nm fumed silica particles. Each plot includes two curves for the epoxy with the largest and smallest epoxy strengths that were recorded [1].

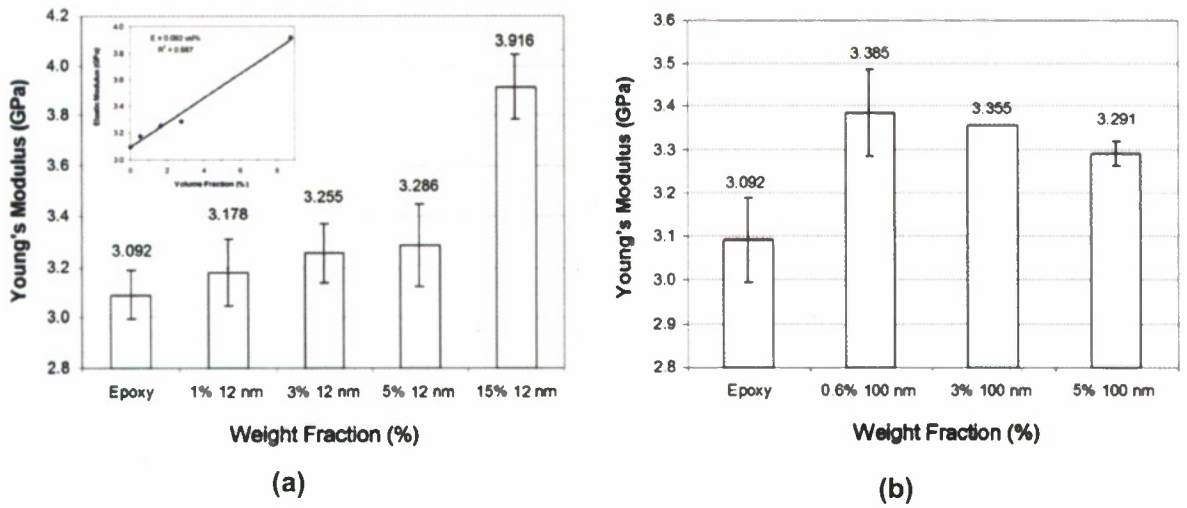

Figure 3. Young's moduli of composites with **(a)** 12-nm, and **(b)** 100-nm fumed silica particles as a function of particle weight fraction [1].

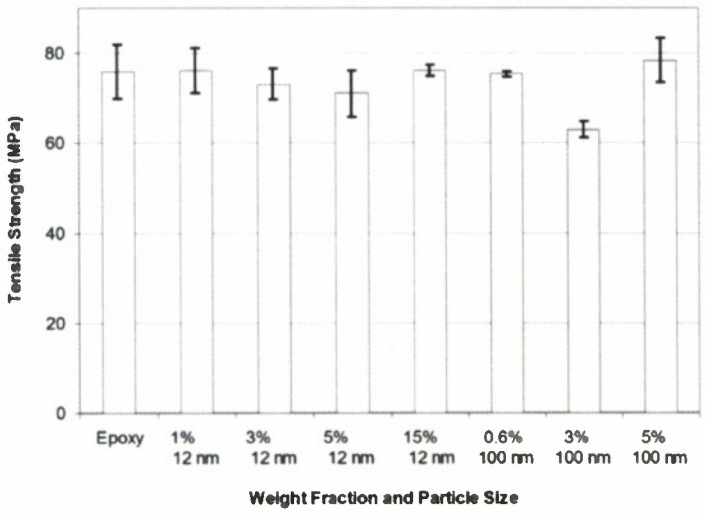

Figure 4. Tensile strength of 12-nm and 100-nm silica particle composites as a function of weight fraction [1].

At 1-3 wt.% the average spacing between secondary particles is large (~500-310 nm), allowing for extended plastic zones in the matrix, and, thus, increased compliance (reduced modulus). Primary particles on the other hand, even at small volume fractions, result in 8 times smaller interparticle spacing which is similar to their size. Small interparticle spacing limits the extent of matrix plasticity and therefore the amount of matrix softening. The composite strengths were rather insensitive to small or large nanoparticles, even at 15 wt.%. Figure 4 shows the ultimate strengths and the standard deviations recorded. While an improvement in strength due to hard particles was not expected, the fact that the tensile strength was not compromised by the hard nanoscale inclusions even at large weight fractions was a positive outcome.

1.3.b. Effective Mechanical Behavior - Fracture Experiments

Figure 5 shows a load-displacement diagram of a fracture experiment. In all fracture tests, the maximum load P_Q was less than 210 N, which corresponded to a far-field stress of 10.5 MPa, which was always within the elastic portion of the stress-strain curves, shown in Figure 3.

The normalized (by the toughness of the epoxy resin which was 1.01±0.01 MPa$\sqrt{m}$) mode I composite fracture toughness increased monotonically with the weight fraction, Figure 6. Small weight fractions (1 wt.%) resulted in 20% increase in the effective toughness, but this improvement was less dramatic at larger weight fractions. For instance, there was marginal difference in toughness between 3 wt.% and 5 wt.% composites, while there was a 35% increase for composites with 15 wt.% particles. These values agree in general with literature data. Also, this saturation in nanocomposite toughness has been reported for all types of hard nanoscale reinforcements, including higher aspect ratio particles [3,4,16]. In fact in some of these reports, the composite toughness dropped at volume fractions larger than 15%.

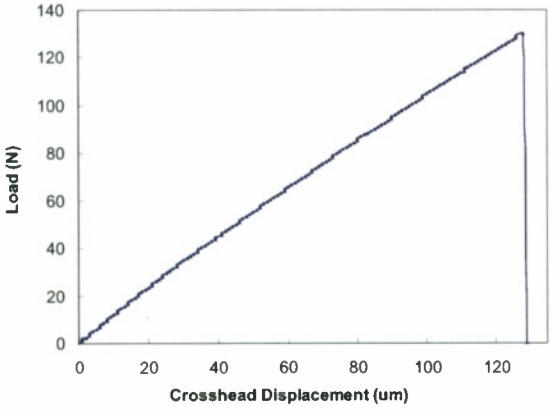

Figure 5. Load-displacement curve from a mode-I quasi-static fracture test for a 15 wt.%, 12-nm silica composite [1].

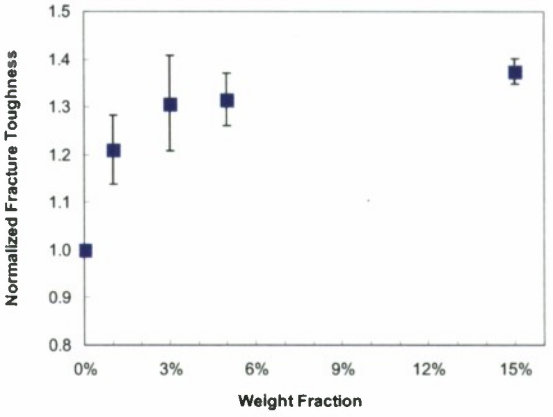

Figure 6. Normalized fracture toughness (with that of the epoxy matrix) as a function of weight fraction of 12-nm silica particles [1].

1.3.c. Local Mechanical Behavior of the Epoxy Matrix

The mechanical behavior of matrix at the scale of nanoparticles was investigated by measurements of local strain in composites with 100 nm particles. In 12-nm particle composites the resolution of the AFM/DIC method was not sufficient to discern the local effect of nanoparticles on the matrix. Figures 7(a,b) show the strain field in a 3.0×3.0-μm^2 area in 3 wt.% and 5wt.%, 100-nm particle, composites as obtained by DIC calculations on AFM images recorded during specimen axial loading. The applied uniaxial load was in the direction shown in the figure and resulted in 1% far-field strain. In these figures, the strain fields are superposed on the undeformed AFM image to identify correlations between nanostructure and the local mechanical behavior. The surface protrusions in the gray-scale background are surface particles as detected in the photodetector signal of the AFM.

Although the exact details of nanosphere distribution and density vary locally in each sample, the locations selected for AFM imaging were representative of each weight fraction. In both 3 wt.% and 5 wt.% samples, the strain field in the matrix was highly heterogeneous due to the presence of hard spheres. For the 3 wt.% composite, the matrix strain between nano-particles was as high as 3 times the applied far-field strain at the long strain bands in the matrix that were normal to the applied far field. The width of these bands correlates with the aforementioned interparticle spacing (~310 nm) that was calculated from Equation (1). This local softening was quite pronounced and it reduced composite stiffness. As a consequence, the effective mechanical response of the 3 wt.% composites followed closely that of the control epoxy, as seen in Figure 2(b), since the strain in the matrix was quite higher than the composite strain and therefore the matrix was more compliant than expected.

Figure 7(b) is the superposition of the strain field onto an AFM surface image in a 5 wt.% (100-nm particles) composite at 1% applied strain. Similar conclusions are drawn as in Figure

7(a) in terms of strain heterogeneity. In comparison, the spectrum of strains in 5 wt.% composites was more diverse than in 3 wt.% composites, but strain maxima were in both cases ~3 times the far field. However, the large particle density at 5 wt.% did not allow for the formation of the extensive bands of inelastic strain seen in Figure 7(a). Matrix strain was locally very small near dense particle regions that are marked as *A* in Figure 7(b). Large particle densities resulted in matrix strain shielding or neighboring particles acting collectively as a single large particle, which occurred in regions labeled as *B* in Figure 7(b). Strain localization followed patterns similar to those in Figures 7(a,b) until at least 3% applied strain.

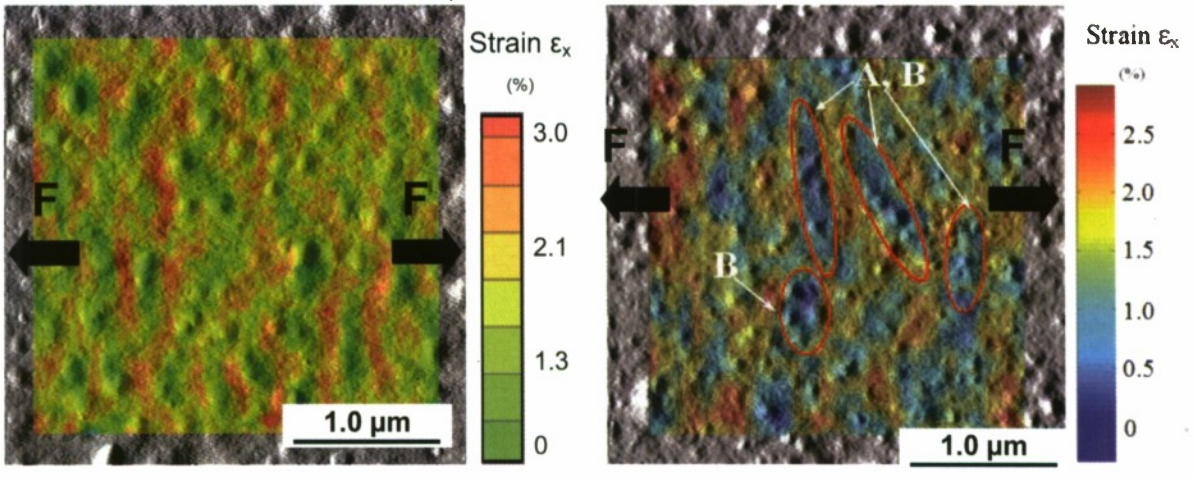

(a) **(b)**

Figure 7. Strain distribution in composites with **(a)** 3 wt.%, and **(b)** 5 wt.%, 100-nm silica at 1% macroscale strain. In **(b)** the contribution of subsurface nanoparticles makes correlations between particle location and strain field less apparent. Contour plots are best viewed in color [1].

The localized damage in 3 wt.% composites correlated well with macroscopic damage accumulation where analogous damage zones of high strain formed prior to microcracking. Actually, strain localization at the sub-millimeter scale followed patterns similar to those at the particle scale, Figure 7(a), and the accumulated damage evolved into microcracks. Contrary to the strong strain inhomogeneity at the scale of the nanofiller, even at strains < 0.3%, the strain distribution at the millimeter scale was relatively uniform until ~0.5% strain.

1.4. Discussion

The local matrix strain distribution in Figure 7 provides a basis for the interpretation of the composite mechanical response in Figures 2(a) and 2(b) where an increase in the particle weight fraction did not result in an improvement in the effective modulus for up to 3 wt.% silica,

as opposed to 5 wt.% and 15 wt.% loadings. The inelastic strain bands in the epoxy matrix at 3 wt.% silica acted almost as "non-linear springs" in series with the particles and the applied load, which imposed the mechanical behavior of the (softened) matrix to the mechanical behavior of the composite. Thus, while the composite was subjected to 1% strain, the matrix had softened locally, and in large zones its stiffness was that at 3% applied strain in the matrix. The difference in matrix stiffness between 1% and 3% was quite large as it can be gathered from Figure 2(b).

At larger particle densities, 5 wt.%, the formation of extended damage zones in the AFM-based measurements was limited by surface and subsurface particles that played an obstructing role in development of large extend of matrix damage. It is expected that a similar strain distribution (perhaps not with exactly the same strain amplitudes) was developed inside the composite. As a consequence, at large strains, the 5 wt.% composite did not demonstrate the same softening that was observed at smaller weight fractions, Figure 2(b). On the other hand, similar damage zones formed at the submillimeter scale (larger than an RVE) which potentially was an evolution of the matrix damage occurring at the scale of the nanoparticles, Figure 7(a). At the scale of the inclusions, this localized deformation became first apparent at strains as small as 0.3%, while at the submillimeter scale, localization of strain was not observed for strains up to 0.5%. Therefore, if these composite fillers are used as matrix replacement in carbon fiber composites with fiber diameters smaller than 10 μm, then the matrix behavior will be highly heterogeneous at the scale of interfiber spacing.

From a molecular viewpoint, large particle weight fractions and small interparticle spacing reduced molecular mobility and therefore strain homogeneity in the matrix. A closer view to the 5 wt.% composite in Figure 7(b) points to regions *A* and *B* where the matrix is at low strain compared to locations with smaller particle densities. The regions of localized strain formed early in the loading history (ε=0.3%) because the silica particles acted as distributed stress raisers. At larger applied strains, specimen areas rich in nanoparticles remained at relatively smaller strain compared to their surroundings while the regions of high strain were still discontinuous compared to the long strain bands in the 3 wt.% composite in Figure 7(a). Such strain localization and reduced load transfer in the matrix has also been discussed in many modeling works, such as that by Sheng *et al.* [5], but this is the first time that is reported from direct experiments.

In terms of matrix toughening, local AFM-based strain measurements were not possible so answers were sought in post-mortem SEM images of the specimen process zones. In conventional epoxy composites, the mechanisms that increase the over-all fracture toughness include filler\matrix debonding and void formation, shear yielding\banding, craze formation, crack deflection, and crack pinning, [6-13]. Recent literature has pointed out that most of these mechanisms dominant in microcomposites may not be important in nanocomposite materials [3,14-16]. Observations on the fracture surface of the epoxy carried out by SEM, see Figure 8(a), showed brittle behavior as characterized by smooth crack surface and, thus, weak resistance to crack propagation. In contrast to the control epoxy, the 15 wt.% nanocomposite process zone fracture surface demonstrated severe micro-roughness, Figure 8(c,d), in the form of surface flakes that provided a tortuous crack surface and local matrix yielding, which aided energy dissipation and, therefore, toughening. The black arrows in Figures 8(b,d) point to 30-50 nm particles, which implies that decohesion occurred between the matrix and an epoxy layer attached to the particles, with thickness comparable to the particle diameter. The white arrows

in Figure 8(d) point to sites of particle debonding but the contribution of particle debonding to matrix toughening was very limited compared to the effect of matrix yielding. At smaller weight fractions, Figure 8(b), particle debonding and void formation (~15 nm) occurred, instead of matrix yielding, which appears to be the only difference in the process zone of the 1-5 wt.% silica composites, compared to the neat epoxy.

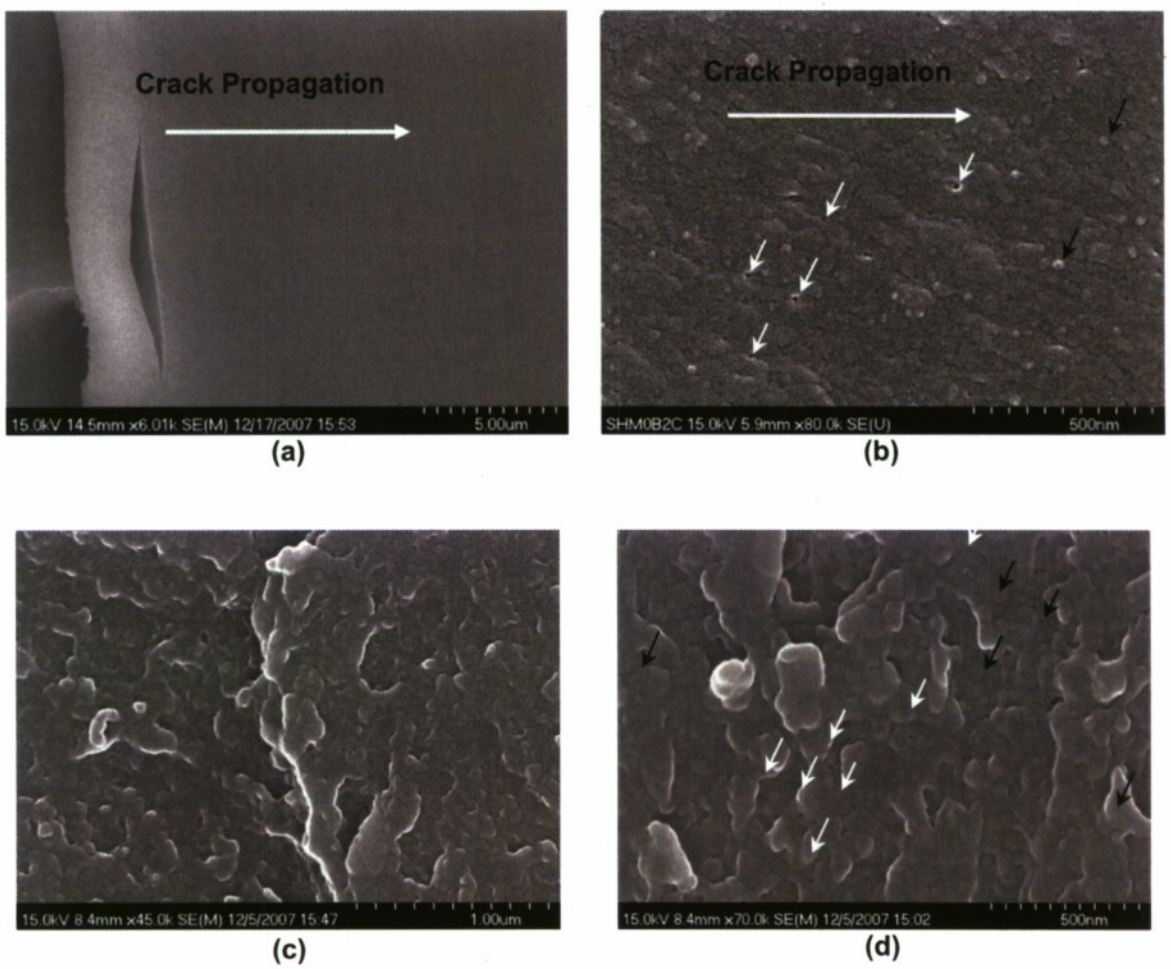

Figure 8. **(a)** Fracture surface at the process zone near the pre-crack tip of the control epoxy, **(b)** of 5 wt.%, and **(c,d)** of 15 wt.% silica composites. The amplitude and lateral extent of surface flakes is considerably larger than the particle size. The white arrows in Figures **(b)** and **(d)** point to voids and the black arrows to surface features that are associated with silica particles surrounded by matrix [1].

2. MECHANICAL AND INTERFACIAL PROPERTIES OF SINGLE VGCNFS

Three different grades of Vapor Grown Carbon Nanofibers (VGCNFs), namely as-fabricated (PR-24-XT PS), high temperature hear treated (PR-24-XT-HHT-LD), and high temperature hear treated and oxidatively treated nanofibers (PR-24-XT HHT-LD-OX) were obtained from Applied Sciences Inc. (Applied Sciences Inc., Ohio) and were tested for their mechanical and interfacial properties in EPON epoxy.

2.1. Mechanical Strength and Failure Behavior of VGCNFs

Table 1 lists the Weibull cumulative probability density function parameters computed for the tensile strength of the different grades of VGCNFs. The experimental results are presented in the form of probability of failure plots in Figures 9(a-c). For two of the three fiber grades, the calculated Weibull moduli were relatively small indicating the presence of a broad spectrum of flaws. The Weibull modulus and strength were calculated by the maximum likelihood function and by linear regression. The agreement between the two methods provides a strong indication that the experimental data sets, although not large in number, were very descriptive of the failure strength distributions of all nanofiber grades [17]. The characteristic strength of pyrolytically stripped (PS) nanofibers based on outer fiber diameter was 3.34 GPa compared to the characteristic strength of 2.84 GPa for the high temperature heat-treated carbon nanofibers (HHT) without an oxidative surface treatment (OX). On the other hand, the effect of oxidative surface treatment on the average fiber strength was less significant than that of the high-temperature heat treatment, as the characteristic strength decreased slightly to 2.74 GPa after surface oxidation (HHT-OX).

Table 1. Weibull parameters, elastic moduli and mean strength for three VGCNF grades [18].

Nanofiber grade	Weibull modulus, m	Characteristic strength, σ_C (GPa)	Elastic modulus, E (GPa)	Average strength (GPa)
PR-24-XT PS	2.4	3.35	180 ± 60	2.90 ± 1.4
PR-24-XT-HHT-LD	7.3	2.85	245 ± 52	2.35 ± 0.4
PR-24-XT HHT-LD-OX	4.4	2.75	-	2.40 ± 0.6

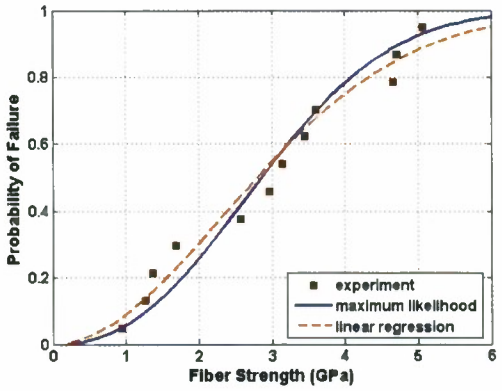

(a)

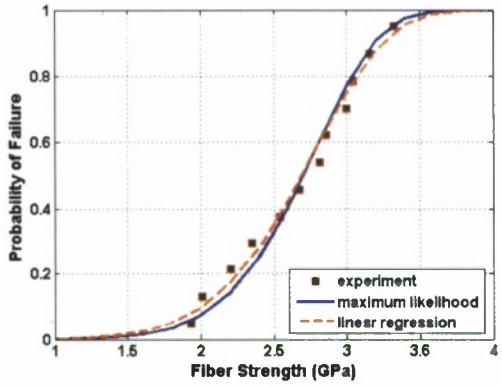

(b)

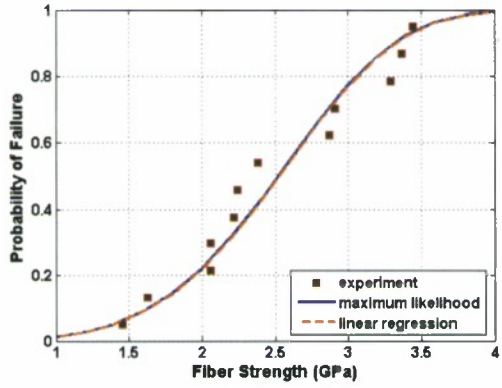

(c)

Figure 9. Probability of failure vs. tensile strength for **(a)** pyrolytically stripped, **(b)** high temperature heat treated, and **(c)** oxidatively processed high temperature heat treated carbon nanofibers [18].

The positive effect of post-fabrication heat treatment on the spread of the tensile strength data was reflected in the higher Weibull moduli of HHT and HHT-OX grades compared to that of the PS grade, as shown in Figure 9, and in the characteristic strength and standard deviation values in Figure 10. The present strength analysis considers only the nanofiber outer diameter for the calculation of nominal cross-sectional area of the carbon nanofiber. Since polymer infiltration into the nanofiber inner hollow core is not observed, any physical interaction of the hollow fiber interior with the surrounding matrix is immaterial. Therefore, for all practical purposes, the effective outer fiber diameter is of primary interest. In general, the diameter of the hollow core is about ½ that of the outer fiber diameter [19]. Consequently, the true fiber strength is ~33% higher than that reported here. In this regard, the high values of the true fiber strength are similar to that of high strength microscale carbon fibers [20,21].

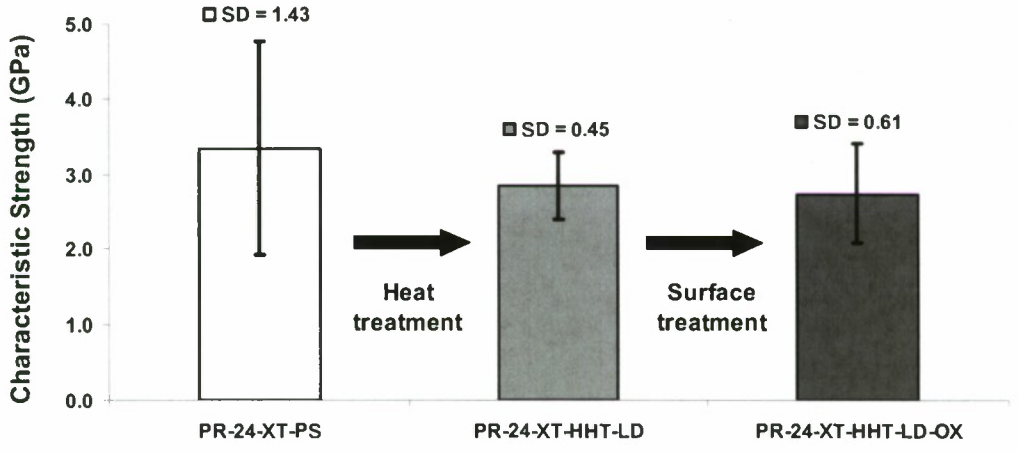

Figure 10. Characteristic strength for three VGCNF grades. The error bars correspond to one standard deviation [18].

In an analogy to conventional carbon fibers, for instance see Lake et al. [22], the decrease in the scatter of the tensile strength values from PS to the HHT grade can be explained by the transformation of the turbostratic layer to a graphitic layer that is coaxial to the fiber, as opposed to the inner graphitic shell that pre-existed the heat treatment. According to Endo et al. [23], high-temperature heat treatment increases the nanofiber structural organization and, therefore, the associated strength uniformity by reducing both the size and the number of micro- and nanoscale defects residing in the catalytically grown graphene layers of the carbon nanofiber inner layer. This improvement is achieved through several thermally induced, microstructural transformations, such as graphitization, decreased interlayer spacing and loop formations between adjacent active edge sites of the oblique graphene cones at the interior and the exterior ends of the nanofiber backbone [23]. Our results for VGCNFs are in agreement with existing literature, where an increase in the graphitization temperature decreases the fiber

strength. According to [22], this is due to the reduction of the load bearing turbostratic layer and the increase of the ordered graphene planes. Such structural transformations occur at the expense of the vapor deposited turbostratic carbon layer, as shown in the TEM pictures in Figures 11(a,b). Similar to microscale carbon fibers, the turbostratic outermost carbon layer in pyrolytically stripped VGCNFs tends to inhibit crack propagation due to misorientation of neighboring graphitic planes which limits transverse crack propagation during fracture and hence increases the fracture resistance of the overall fiber structure [21]. The mechanical benefit of the turbostratic carbon layer is owed to its coaxial orientation with respect to the nanofiber, while the catalytically grown inner graphene layers are oriented obliquely with respect to the nanofiber axis as shown in Figure 11(a).

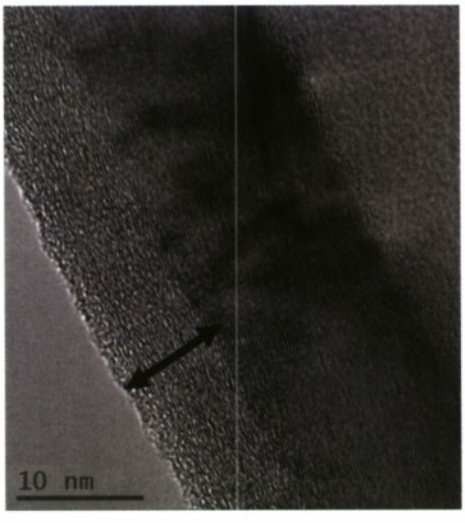

(a)

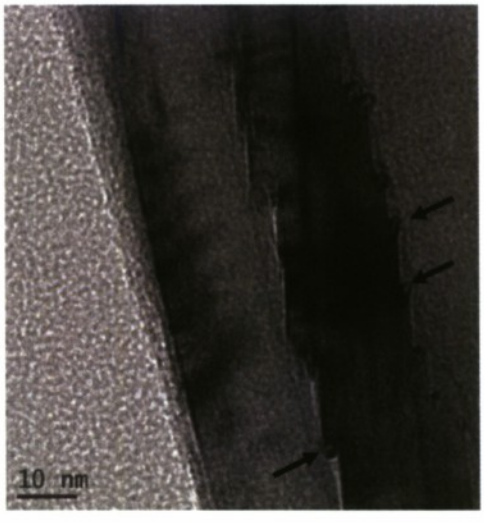

(b)

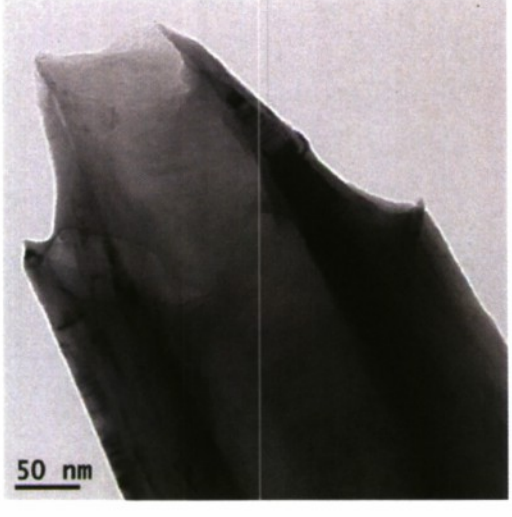

(c)

Figure 11. TEM images of **(a)** pyrolytically stripped, and **(b,c)** high temperature heat treated VGCNFs. The turbostratic carbon layer is shown with the double sided arrow in **(a)** followed by a (dark) graphitic layer and the (gray) hollow fiber core. The turbostratic carbon layer is reduced after heat treatment as shown in **(b)** where the dark band is the hollow fiber core. Heat treatment is responsible for the interior and exterior edge loops (shown with single sided arrows) in **(b). (c)** Nanofiber failure section with a protruding inner cone due to graphene layer sliding [18].

From a mechanics point of view, it is clear that the ultimate load-bearing capacity of this hybrid structural arrangement would reach its maximum for a structure that is solely comprised of parallel-oriented graphene layers, as can be inferred from continuum elasticity models and molecular dynamics (MD) simulations [24,25]. Thus, the experimentally recorded reduction in the strength of the graphitized (heat treated) nanofibers can be explained on the basis of load transfer from the outer layer to the inside graphitic layer.

SEM and TEM fractography revealed mutual sliding of graphene planes following the cleavage failure of the outer fiber shell, as shown in Figures 11(c) and 12(a,c). In the as-fabricated fibers, failure initiated in the outer fiber layer with subsequent sliding of the inner graphitic layer. The outer layer is aligned in the fiber direction and, therefore, it is subjected to higher stresses compared to the oblique inner graphitic layer since both layers experience the same strain (isostrain condition). Since the outer layer is more defect prone than the inner layer due to its turbostratic nature, fracture is expected to begin in the former where carbon is also more disorganized and crack paths can easily form.

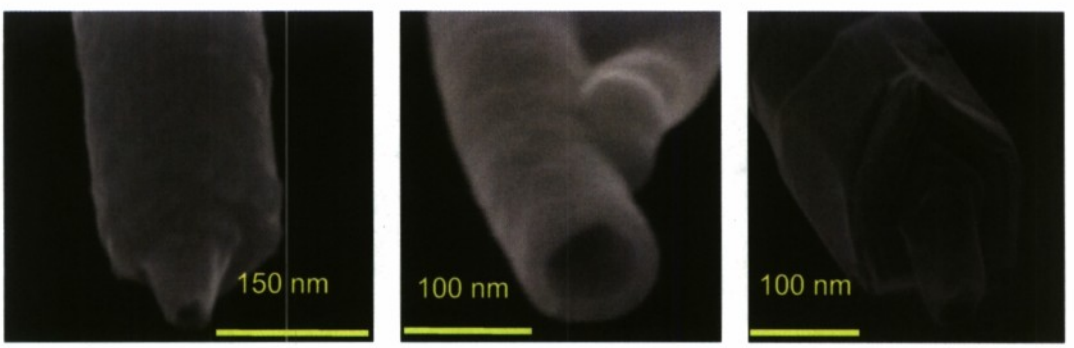

Figure 12. Rupture surfaces of **(a)** PS, **(b)** HHT-OX, and **(c)** HHT-LD VGCNFs. The fiber fracture profile includes evidence of sliding of the inner graphene planes which is owed to the stacked truncated cone structure of the nanofibers [18].

On the other hand, in HHT and HHT-OX fibers the outer turbostratic layers have been converted into graphitic during heat treatment process but the re-organization of the oblique inner graphitic layer resulted in the serrated (truncated cone) structure in the nanofiber core, as pointed out by the arrows in Figure 11(b). These steps may also serve as stress concentrations and sites of failure initiation which proceeds with sliding of the graphene planes. However, since the outer graphitic layer determines the fiber strain (it is stiffer than the inner layer and therefore it experiences higher stresses than the inner layer) it is expected that failure initiation still occurs in that the outer layer due to its surface flaws. This mode of failure was observed in the majority of the failed fiber cross-sections, as shown in Figure 12.

In comparison with the few literature data on VGCNF strength, the nanofiber strengths measured in this study were obtained from the thinnest fibers tested individually to date; they

were on average 50% thinner than the smallest fibers tested in [26]. The strength of the thinnest fibers in the last reference was at most 2 GPa, while the majority of fiber strength values reported in [26] were in the 500-1000 MPa range for nanofiber diameters between 300-1000 nm. The authors showed a significant diameter size effect on the mechanical strength of their nanofibers and a rapidly increasing strength for diameters ~300 nm. Their reported trends in fiber strength could actually predict the considerably higher nanofiber strengths presented here. On the other hand, the only other literature report on VGCNF strength [27] provided a nanofiber strength value of 2.92 GPa, which is very similar to the average fiber strengths measured in this paper. The latter fibers were grown to micron scale diameters by the same commercial process that furnished the fibers tested in this work. However, the fact that the strength of VGCNFs from the same fabrication process does not appear to change with fiber diameter potentially points out to surface defects in the fibers that are not scalable with fiber size. Nevertheless, this disagreement between the strengths reported in references [26] and [27] points out to the need for experiments every time a new fabrication method is developed, or modifications to an existing fabrication process are introduced, especially if nanostructured materials are concerned.

2.2. Elastic Modulus of Nanoscale VGCNFs

In order to obtain a reliable estimate of the elastic modulus for the investigated VGCNFs, a new MEMS device was developed that was manufactured from polycrystalline silicon using the Sandia National Laboratories' SUMMIT™ process. Since the effect of heat treatment on the value of the elastic modulus is of primary interest, experimental priority was given to the high-temperature-heat-treated PR-24-HHT-LD grade of VGCNFs.

A representative optical microscopy image of a VGCNF during an experiment and the stress-strain curve calculated by considering only the outer fiber diameter are given in Figures 13(a-b). In modulus experiments, the strain resolution depends on the length of the nanofibers, therefore, it was attempted to select long and straight fibers. In order to prevent sliding at the grips or compliant fixtures due to the epoxy adhesive, the fibers were fixed with a 2-μm thick platinum layer deposited with the aid of a Focused Ion Beam (FIB). The mechanical response of the carbon nanofiber in Figure 13(b) has an initial exponential profile followed by a linear behavior. The best fit line of the latter is the fiber stiffness which is acquired once the fiber is completely stretched. The initial non-linear behavior is attributed to the small bending stiffness that the nanofiber possesses.

The elastic moduli that were obtained in this work (180±60 GPa for pyrolytically stripped and 245±52 GPa for high temperature heat treated) are higher than those obtained by simple AFM-based bending experiments [28]. The much lower values and the large scatter in the moduli reported in [28] could be explained by the small slope of the initial segment of the stress-strain curve in Figure 13(b) where until the fiber is completely stretched, which requires several tens of μN of force, the effective fiber stiffness is significantly smaller than the fiber elastic modulus. This implies that, even when fully aligned, unless significant stress is applied to VGCNFs to remove their initial tortuosity, these fibers do not contribute to the composite stiffness with their true stiffness. The experiments reported in [28] were conducted via bending

of VGCNFs with AFM probes that provide limited force capacity which is not enough to perfectly straighten the nanofibers. Therefore, the modulus measurements presented here are more reliable than the bending experiments reported before.

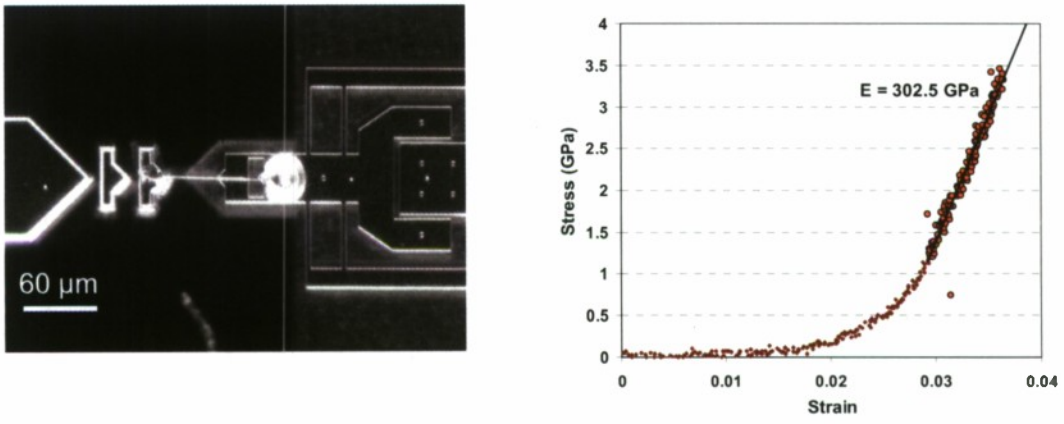

(a) (b)

Figure 13. (a) Image of a stretched VGCNF taken during an experiment. **(b)** Stress-strain curve recorded starting at a loose fiber configuration. The slope of the linear fit of the last portion of the data points (shown in filled circles) corresponds to the elastic modulus [18].

2.3. Interfacial Shear Strength of Individual VGCNFs in Epoxy

A new experimental methodology has been developed to carry out nanoscale pull-out experiments. As the first step in the development process, a parametric design analysis was performed to determine the feasible values for embedded nanofiber lengths considering the fiber strength data obtained previously for investigated carbon nanofibers. Considering the results of this analysis, our efforts were concentrated on achieving precise embedded fiber lengths within 500-2,000 nm range and controlling the profile of the epoxy to satisfy proper embedment conditions for a valid pull-out experiment [29]. Key in this development was the use of microfabricated force sensors using Sandia National Laboratories' SUMMIT™ technology. Considering the relatively high interfacial shear strength (IFSS) value of around 45 MPa obtained from a "proof of concept" experiment with a PR-24-XT-HHT-LD grade carbon nanofiber embedded in a common aerospace grade composite matrix, namely the Epon™ 828 difunctional bisphenol A/epichlorohydrin derived liquid epoxy resin compounded with EPIKURE™ 3140 polyamide curing agent, it was found that embedded fiber lengths of up to 2-3 μm could be used in intended pull-out experiments to quantify the IFSS.

The nanofiber pull-out experiments were executed with a double-column folded beam loadcell, whose true stiffness was determined by a traceable experimental calibration process

based on hanging glass beads of known weight on the loadcell and measuring the corresponding deflection by means of DIC. In terms of the pull-out experiments, the actuation of the nanofiber IFSS apparatus and the data acquisition were performed similarly to the methodology utilized for fiber strength experiments. The ultimate loadcell deflection required to determine the IFSS was resolved by DIC for submicron pixel resolution. Post-mortem images of the remaining pull-out channel and the debonded fiber were taken with an SEM to measure the embedded fiber length, the fiber diameter, and to determine the type of interfacial failure, i.e. adhesive, cohesive or mixed, that occurred during the experiments.

2.4. Results and Discussion

The experimental results obtained by the above described method were analyzed according to three different approaches commonly employed in micromechanics of fiber reinforced composites, namely the maximum shear stress criterion with linearly decaying shear stress (LDSSC), the Chua-Piggott criterion (CPC), and the uniform interfacial yielding based criterion (UIYC) [30,31]. For the calculation of the IFSS according to the Chua-Piggott criterion, following material properties are used: 2.89 GPa [32], E_f = 250 GPa and v_m = 0.35 [30]. The LDSSC and CPC criteria gave very similar results because both criteria were based on the assumption that the maximum shear stress initiated failure of the interface. The UIYC criterion resulted in IFSS values which were 50% of those calculated by LDSCC.

The measured pull-out force was normalized with respect to the nanofiber diameter and is plotted in Figure 14 vs. the embedded fiber length to calculate the average IFSS. In all plots it is clear that the calculated IFSS is independent of the embedded fiber length which implies that the transition region near the edge singularity is rather short. The as-fabricated VGCNFs, Figure 14(a), resulted in high IFSS (111±32 MPa) which was reduced by a factor of two (66±10 MPa) when the nanofibers were heat treated, as shown in Figure 14(b). Therefore, hear treatment had a severe effect on the fracture toughness of composites with embedded VGCNFs. This agrees with composite level experiments reported before where high temperature heat treated nanofibers embedded in epoxies resulted in smaller moduli. When this reduction in IFSS is combined with the smaller tensile strength of the high temperature heat treated nanofibers, it is evident that the composite toughness will be reduced compared to as-fabricated nanofibers. Subsequent surface functionalization resulted in significantly larger IFSS (214±10 MPa), Figure 14(c), which also correlated with improved fracture toughness in composite systems.

In order to obtain further understanding of the process of interfacial failure, which also affects the precision and applicability of the aforementioned models, post-mortem images of the debonded fiber channels and the fibers themselves were taken with an SEM. The pull-out channels had approximately round entry holes without substantial matrix plasticity at the hole circumference. Furthermore, no significant traces of matrix could be detected in the section of the nanofiber that was embedded in the matrix. In almost all cases, the pulled-out section of the nanofiber was clean and smooth, pointing to the adhesive (i.e. non-cohesive) interface failure, with crack initiation and progression happening on the fiber surface.

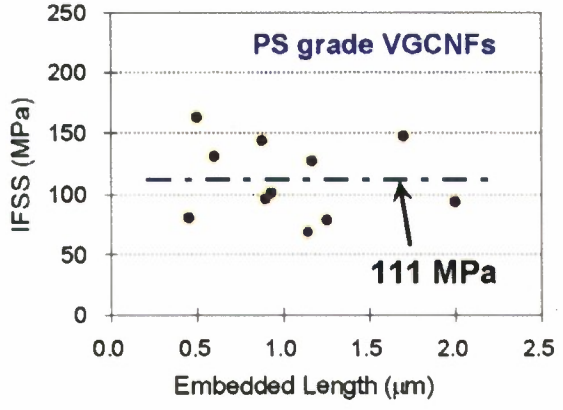

(a)

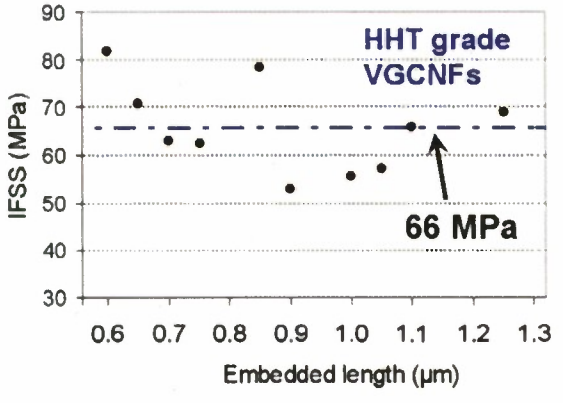

(b)

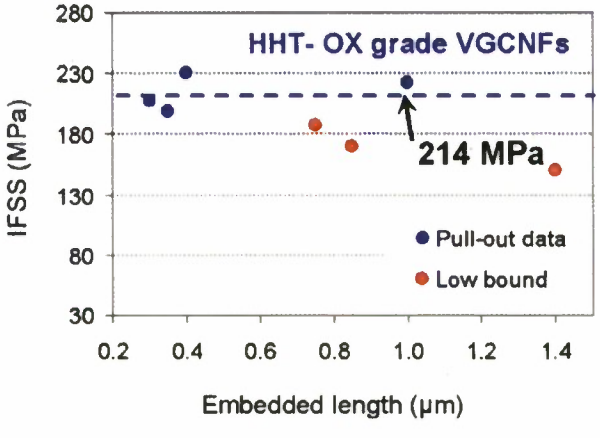

(c)

Figure 14. IFSS vs. nanofiber embedded length for **(a)** as-fabricated, **(b)** high-temperature-heat-treated and **(c)** functionalized high-temperature-heat-treated VGCNFs.

In comparison with the very limited literature data on the IFSS between MWCNTs and epoxy matrices, varying in the wide range between 20-376 MPa [33-35], the experimentally determined IFSS in this study for as-fabricated VGCNFs of 111±32 MPa is significantly more consistent compared to prior works. Therefore, the presented method is considerably more reliable than prior attempts to quantify the interfacial mechanics of individual nanostructures in epoxies. The decrease in the IFSS with increasing nanofiber diameter in our data was much less pronounced than the case of CNTs [33,36], which could be attributed to the growing region of the stress singularity at the fiber entrance point for increasing nanofiber diameter.

3. CONCLUSIONS

In the first component of this AFOSR supported program, the elastic and failure properties (strength and toughness) of fumed silica epoxy nanocomposites were determined. The results, when possible, were augmented by local strain measurements by the AFM/DIC method to identify the physical processes that control and limit the improvement in stiffness and strength in nanostructured materials [1]. In terms of deformation mechanics, the distribution of strain was rather uniform at the scale of the RVE and at strains of up to ~0.5%. However, the distribution of strain was strongly inhomogeneous at the scale of nanoparticles, both in the elastic and the inelastic regimes. For example, at 1% far-field strain, the matrix strain was locally as high as 3%. This matrix strain inhomogeneity and the interaction between adjacent nanoparticles resulted in local matrix strain shielding, and in other regions in early matrix yielding. Due to this large strain inhomogeneity in the matrix, micromechanical models may not provide accurate estimates of the effective properties of this class of nanocomposites. Due to strain localization in the matrix, the composite stress-strain curves of 1-3 wt.% silica did not vary from the matrix. At larger weight fractions, particle density prevented the formation of extensive matrix yielding and resulted in overall stiffening in the stress-strain behavior. The mechanical strength, on the other hand, did not vary appreciably with particle weight fraction and size. No particle debonding was observed in any of the *in situ* tensile tests, while local matrix yielding recorded in the AFM/DIC experiments hinted that failure initiated in the matrix, which in turn, helped to maintain the strength of the neat epoxy. Finally, the fracture toughness of 12-nm silica composites was found to increase by 35% for 15 wt.% silica, compared to neat epoxy. The rate of increase in crack resistance was the highest at small weight fractions (<1 wt.%). Examination of the fracture process zone showed significant roughening significant matrix yielding for the largest particle density, and void formation at all smaller weight fractions.

In the second part of this project a series of novel experiments were conducted to measure for the first time the tensile strength and modulus of individual VGCNFs and to determine their IFSS in EPON epoxy. In all cases, the mechanical behavior was corroborated with detailed SEM and TEM images of the nanofiber structure and the surface of the debonded VGCNF segments. In terms of tensile strength experiments, the nominal tensile strengths of the nanofibers followed Weibull distributions with characteristic strength values in the range of 2.74 - 3.34 GPa, which quantitatively delineated the effect of post-fabrication treatments and associated microstructural transformations on the fiber strength. As-grown nanofibers had

relatively small Weibull modulus indicating the presence of a wide flaw population, which was significantly reduced upon high temperature heat treatment as evidenced by the 230 % increase in the value of the Weibull modulus. These strength values are the first obtained in literature [18] and are 50% or smaller than the previously estimated (from data on macroscale carbon fibers) values commonly reported for VGCNFs. Fractography of the nanofiber rupture region revealed that the stacked, truncated, cup structure of the oblique graphene layers comprising the backbone of VGCNFs is retained during the rupture process. Cleavage of the outer turbostratic layer occurred first, followed by relative slip of the internal oblique graphene layers, indicating the limited participation of the stronger sp^2-bonds in the (discontinuous) graphene basal planes during fiber fracture. A 16% decrease in the mechanical strength (Weibull strength) occurred for the high-temperature-heat-treated nanofibers, which correlated well with TEM images, showing the graphitization of the outer turbostratic layer and the evolution of its interface with the inner, originally graphitic, layer with attendant structural discontinuities that reduced the total load bearing capacity of the nanofibers.

The IFSS of individual VGCNFs in EPON epoxy was quantified by novel nanoscale pull-out experiments. The IFSS for as-fabricated nanofibers was 111±32 MPa pointing out that the bonding of the heat-treated, non-functionalized and non-oxidized carbon nanofiber grade (PR-24-HHT-LD) to the Epon 828/Epikure 3140 epoxy matrix can be better than that of micron size carbon fibers with IFSS values between 40-65 MPa. Compared to the few literature data on the IFSS between MWCNTs and epoxy matrices [34], the experimentally determined IFSS of 214±10 MPa for the functionalized VGCNF-epoxy system is significantly larger than the maximum value of 140 MPa reported for chemically functionalized MWCNTs. Similarly, the IFSS of as-fabricated VGCNFs it also is quite higher than the IFSS value of 30 MPa reported for non-functionalized, pristine MWCNTs. Although the literature measurements with MWCNTs do not meet macroscale standards for accurate and reliable experimental mechanics, these differences in the IFSS values could also be due to defects residing on carbon nanofibers, which promote increased interfacial interactions and therefore result in larger IFSS compared to MWCNTs.

REFERENCES

1. Q. Chen, I. Chasiotis, C. Chen, A. Roy, "Nanoscale and Effective Mechanical Behavior and Fracture of Silica Nanocomposites," *Composites Science and Technology* **68** (15-16), pp. 3137-3144, (2008).
2. P.P. Bansal, A.J. Ardell, "Average near-neighbor distances between uniformly distributed finite particles", *Metallography* **5**, pp. 97, 1972.
3. A.J. Kinloch, A.C. Taylor, "The mechanical properties and fracture behaviour of epoxy-inorganic micro- and nano-composites", *Journal of Materials Science* **41**, pp. 3271, 2006.
4. A.J. Kinloch, R.D. Mohammed, A.C. Taylor, C. Eger, S. Sprenger, D. Egan, "The effect of silica nanoparticles and rubber particles on the toughness of multiphase thermosetting epoxy polymers", *Journal of Materials Science* **40**, pp. 5083, 2005.
5. N. Sheng, M.C. Boyce, D.M. Parks, G.C. Rutledge, J.I. Abes, R.E. Cohen, "Multiscale micromechanical modeling of polymer/clay nanocomposites and the effective clay particle", *Polymer* **45**, pp. 487, 2004.
6. A.C. Roulin-Moloney, Fractography And Failure Mechanisms of Polymers and Composites Elsevier Applied Science, London, 1989
7. F. Heutling, H.E. Franz, K. Friedrich, "Photomicrographic fracture analysis of the delamination propagation in cyclic loaded thermosetting carbon fiber-reinforced composites", *Materialwissenschaften und Werkstofftechnik* **29**, pp. 239, 1998.
8. J. Lee, A.F. Yee, "Inorganic particle toughening I- micro-mechanical deformations in the fracture of glass bead filled epoxies", *Polymer* **42**, pp. 577, 2001.
9. F.F. Lange, "The interaction of a crack front with a second-phase dispersion", *Philosophical Magazine* **22**, pp. 983, 1970.
10. A.G. Evans, "The strength of brittle materials containing second phase dispersions", *Philosophical Magazine* **26**, pp. 1327, 1972.
11. A.S. Argon, R.E. Cohen, "Toughenability of Polymers", *Polymer* **44**, pp. 6013, 2003.
12. K.T. Faber, A.G. Evans, "Crack deflection processes - I. Theory", *Acta Metallurgica* **31**, pp. 565, 1983.
13. K.T. Faber, A.G. Evans, "Crack deflection processes - II. Experiment", *Acta Metallurgica* **31**, pp. 577, 1983.
14. B. Wetzel, F. Haupert, M.Q. Zhang, "Epoxy nanocomposites with high mechanical and tribological performance", *Composites Science and Technology* **63**, pp. 2055, 2003.
15. B. Wetzel, P. Rosso, F. Haupert, K. Friedrich, "Epoxy nanocomposites – fracture and toughening mechanisms", Engineering Fracture Mechanics 73, pp. 2375, 2006.

16. B.B. Johnsen, A.J. Kinloch, R.D. Mohammed, A.C. Taylor, S. Sprenger, "Toughening mechanisms of nanoparticle-modified epoxy polymers", *Polymer* **48**, pp. 530, 2007.

17. J.D. Sullivan, P.H. Lauson, "Experimental probability estimators for Weibull plots", *Materials Science Letters*, **5**(12), pp.1245-1247, 1986.

18. T. Ozkan, M. Naraghi, I. Chasiotis, "Mechanical Properties of Vapor Grown Carbon Nanofibers," *Carbon* **48**, pp. 239-244, 2010.

19. D. Burton, P. Lake, G. G. Tibbetts, M. L. Lake, "Novel applications of carbon nanofibers", *SAMPE Journal* **43**(4), pp. 36-40, 2007.

20. P. Morgan, Carbon Fibers and Their Composites, CRC Press, Boca Raton, FL, pp. 27-41, 2005.

21. J.G. Lavin, Fracture of Carbon Fibers, In: M. Elices, J. Llorca, editors, Fiber Fracture, Elsevier Science, Oxford, UK, pp. 157-179, 2002.

22. M.L. Lake, D.G. Glasgow, C. Kwag, D.J. Burton, "Carbon nanofiber polymer composites: electrical and mechanical properties", Proceedings, Affordable Materials Technology: 47th International SAMPE Symposium and Exhibition, Society for the Advancement of Material and Process Engineering, Long Beach (CA USA), pp. 1794-1800, 2002.

23. M. Endo, Y. A. Kim, T. Hayashi, T. Yanagisawa, H. Muramatsu, M. Ezaka, H. Terrones, M. Terrones, M. S. Dresselhaus, "Microstructural changes induced in "stacked cup" carbon nanofibers by heat treatment", *Carbon* **41**(10), pp. 1941-1947, 2003.

24. C. Wei, D. Srivastava, "Nanomechanics of carbon nanofibers: Structural and elastic properties", *Applied Physics Letters* **85**(12), pp. 2208-2210, 2004.

25. J.X. Wei, K.M. Liew, X.Q. He, "Mechanical properties of carbon nanocones", *Applied Physics Letters* **91**(26), pp. 261906, 2007.

26. M. Endo, Y.A. Kim, T. Hayashi, K. Nishimura, T. Matusita, K. Miyashita, M.S. Dresselhaus, "Vapor-grown carbon fibers (VGCFs) Basic properties and their battery applications", *Carbon* **39**(9), 1287-1297, 2001.

27. G.G. Tibbetts, J.J. McHugh, "Mechanical properties of vapor-grown carbon fiber composites with thermoplastic matrices", *Journal of Materials Research* **14**(7), pp. 2871-2880, 1999.

28. J. G. Lawrence, L. M. Berhan, A. Nadarajah, "Elastic properties and morphology of individual carbon nanofibers", *ACS Nano* 2 (6), pp. 1230-1236, 2008.

29. P.J. Herrera-Franco, L.T. Drzal, "Comparison of methods for the measurement of fiber/matrix adhesion in composites", *Composites* **23**, pp. 2-27, 1992.

30. L.T. Drzal, P.J. Herrera-Franco, "Measurement methods for fiber-matrix adhesion in composite materials", In: The Mechanics of Adhesion, D. A. Dillard and A. V. Pocius (editors), Elsevier Science B. V., Amsterdam, The Netherlands, pp. 605-660, 2002.

31. P.S. Chua, M.R. Piggott, "The glass fibre-polymer interface. I. Theoretical considerations for single fibre pull-out tests", *Composites Science and Technology* **22**, pp. 33-42, 1985

32. Hexion Specialty Chemicals, "EPIKURE Curing Agent 3140", Technical Data Sheet, pp. 1-4, Re-issued August 2007, available at: www.hexion.com

33. C.A. Cooper, S.R. Cohen, A.H. Barber, H.D. Wagner, "Detachment of nanotubes from a polymer matrix", *Applied Physics Letters* **81**(20), pp. 3873-3875, 2002.

34. A.H. Barber, S.R. Cohen, S. Kenig, H.D. Wagner, "Interfacial fracture energy measurements for multi-walled carbon nanotubes pulled from a polymer matrix", *Composites Science and Technology* **64**(15), pp. 2283–2289, 2004.

35. J. Gou, B. Minaie, B. Wang, Z. Liang, C. Zhang, "Computational and experimental study of interfacial bonding of single-walled nanotube reinforced composites", *Computational Materials Science* **31**, pp. 225-236, 2004.

36. Y. Ganesan, J. Lou, "The mechanical characterization of carbon-nanotube-reinforced-polymer-matrix nanocomposites: An unfolding story of interface", *JOM* **61**(1), pp. 32-37, 2009.